Direct Microwave Measurement of Andreev-Bound-State Dynamics in a Semiconductor-Nanowire Josephson Junction

M. Hays,[1,*] G. de Lange,[1,2,3] K. Serniak,[1] D. J. van Woerkom,[2,3] D. Bouman,[2,3] P. Krogstrup,[4]
J. Nygård,[4] A. Geresdi,[2,3] and M. H. Devoret[1,†]

[1]*Department of Applied Physics, Yale University, New Haven, Connecticut 06520, USA*
[2]*QuTech and Delft University of Technology, 2600 GA Delft, Netherlands*
[3]*Kavli Institute of Nanoscience, Delft University of Technology, 2600 GA Delft, Netherlands*
[4]*Center for Quantum Devices and Station Q Copenhagen, Niels Bohr Institute, University of Copenhagen,
Universitetsparken 5, 2100 Copenhagen, Denmark*

The modern understanding of the Josephson effect in mesosopic devices derives from the physics of Andreev bound states, fermionic modes that are localized in a superconducting weak link. Recently, Josephson junctions constructed using semiconducting nanowires have led to the realization of superconducting qubits with gate-tunable Josephson energies. We have used a microwave circuit QED architecture to detect Andreev bound states in such a gate-tunable junction based on an aluminum-proximitized indium arsenide nanowire. We demonstrate coherent manipulation of these bound states, and track the bound-state fermion parity in real time. Individual parity-switching events due to nonequilibrium quasiparticles are observed with a characteristic timescale $T_{\mathrm{parity}} = 160 \pm 10 \ \mu$s. The T_{parity} of a topological nanowire junction sets a lower bound on the bandwidth required for control of Majorana bound states.

The fundamental process governing the physics of mesoscopic superconductors is Andreev reflection, whereby electrons are coherently scattered into holes due to spatial variation of the superconducting order parameter [1]. Within a Josephson junction conduction channel, Andreev reflection processes constructively interfere to form localized fermionic modes known as Andreev bound states (ABS). These modes have energies less than the superconducting gap, and are responsible for the flow of the Josephson supercurrent [2,3]. While the phenomenological properties of Josephson junctions are widely utilized in superconducting circuits [4–6], they can only be understood in detail by considering the underlying ABS.

Here we outline the physics of the lowest-energy ABS of a Josephson junction, which is spin degenerate with energy E_A assuming time-reversal invariance [Fig. 1(a)]. The many-body configurations of this level can be separated into two manifolds indexed by the parity of fermionic excitations. The even-parity manifold is spanned by the ground state $|g\rangle$ and doubly excited state $|e\rangle$, while the odd-parity manifold is spanned by the singly excited spin-degenerate states $|o\downarrow\rangle$ and $|o\uparrow\rangle$. As the parity-conserving $|g\rangle \leftrightarrow |e\rangle$ transition involves only discrete subgap levels, the even manifold is amenable to coherent manipulation by microwave fields at frequency $f_A = 2E_A/h$ [7–10]. We thus refer to the even manifold as the Andreev qubit. Dynamics between the even and odd manifolds cannot be controlled, as parity-breaking transitions result from incoherent quasiparticle exchange

with the continuum of modes in the junction leads [11–13]. However, it is possible to observe these quasiparticle poisoning events by tracking the ABS fermion parity in real time. The ABS can therefore act as a single-particle detector of the nonequilibrium quasiparticles that plague superconducting devices [14–19]. Experiments revealing these dynamics have been performed on ABS hosted by superconducting atomic contacts [10,11].

Advances in the fabrication of superconductor-proximitized semiconducting nanowires [20,21] have enabled reliable construction of highly transparent nanowire Josephson junctions (NWJJ). Because of the low carrier density of semiconductors, the conduction channels of NWJJs can be tuned *in situ* by electrostatic gates, providing convenient control over the ABS [22,23]. Such control has been used to create gate-tunable Josephson elements for superconducting quantum circuits [24,25]. Moreover, high-spin-orbit, large-g-factor NWJJs can, in principle, be tuned into a topological phase in which the lowest-energy ABS evolves into a Majorana bound state (MBS) [26,27]. As poisoning by nonequilibrium quasiparticles will hinder efforts to probe the physics of MBS [28], monitoring the fermion parity switches of the precursor ABS is a first step towards understanding and mitigating poisoning in a topological NWJJ.

In this Letter, we report the microwave detection and manipulation of ABS in an aluminum-proximitized indium arsenide (InAs) NWJJ using circuit quantum
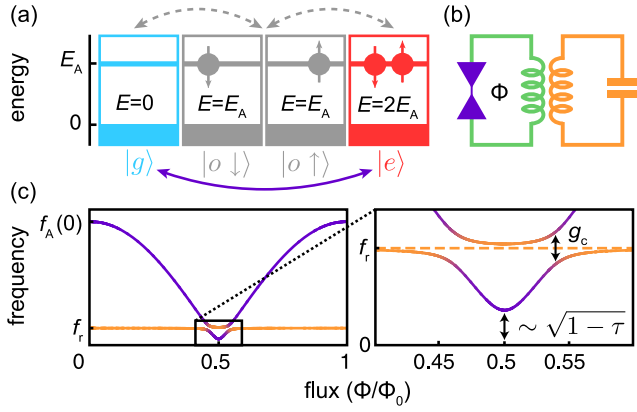
FIG. 1. Model of ABS coupled to a microwave resonator. (a) Many-body configurations of a spin-degenerate Andreev level in the excitation representation. A microwave transition (purple arrow) links $|g\rangle$ and $|e\rangle$, while quasiparticle poisoning (gray dashed arrows) links the even and odd manifolds. (b) A NWJJ (purple) inductively coupled to microwave readout resonator (orange) via a superconducting loop (green). An externally applied flux Φ phase biases the NWJJ. (c) A representative spectrum of the system consists of $f_A(\Phi)$ (purple) and the resonator transition (orange). The maximum of f_A occurs at $\Phi = 0$ and depends on the geometric and material properties of the NWJJ. Enlargement: the minimum of $f_A(\Phi)$ occurs at $\Phi = \Phi_0/2$ and is determined by the channel transparency τ. The Andreev qubit is coupled with strength g_c to the resonator mode, while the odd manifold is decoupled leaving only the bare resonator transition (dashed orange line).
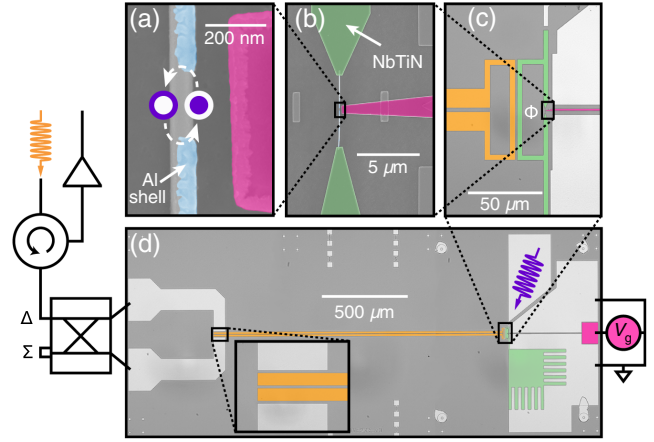

FIG. 2. Color-enhanced device micrographs and simplified experimental setup. (a) Scanning electron micrograph (SEM) of the InAs NWJJ hosting the ABS. The nanowire was partially coated with a 10 nm thick epitaxial Al shell (blue) [21], with a 200 nm gap forming the junction. A NbTiN gate (pink) was used for electrostatic tuning of τ. (b) SEM of the NWJJ contacted by NbTiN leads (green). (c) Optical micrograph of the inductive coupling (strength $g_c/2\pi = 23$ MHz) between the NbTiN loop (green) and the $\lambda/4$ coplanar stripline resonator (orange). The top of the loop was capacitively coupled to a microwave drive line [see panel (d)]. (d) Optical micrograph of the full chip. The resonator was measured using the microwave setup depicted in summary on the left of the figure. A readout tone with frequency f_r (orange arrow) was transmitted through a 180° hybrid, differentially driving the resonator through coupling capacitors (see zoom). The reflected tone was routed through a circulator and amplified before being processed at room temperature. The gate was biased with an electrostatic voltage V_g, with an interdigitated capacitor (green) providing a reference to the device ground plane. A microwave drive (purple arrow) was used to induce transitions between $|g\rangle$ and $|e\rangle$.

electrodynamics (cQED) [29,30]. We perform microwave spectroscopy of a gate- and flux-tunable Andreev qubit, and we achieve coherent manipulation of this qubit using pulsed microwave fields. In addition, we monitor the ABS in real time to directly observe transitions between the even- and odd-parity manifolds, which we attribute to exchange of nonequilibrium quasiparticles between the ABS and the junction leads. These parity-switching events are observed to occur with a characteristic timescale $T_{\mathrm{parity}} = 160 \pm 10$ μs.

Our cQED detection scheme hinges on the supercurrent properties of the ABS. While the even manifold supports the flow of supercurrent, the odd manifold does not. To probe the ABS of a NWJJ, we therefore inductively coupled the junction to a superconducting microwave resonator with bare frequency f_r [Fig. 1(b)] [10]. With the system tuned such that the magnitude of $\Delta = 2\pi(f_A - f_r)$ is much greater than the coupling strength g_c, the interaction between the resonator and the current-carrying Andreev qubit is well described by a dispersive coupling term in the Hamiltonian $\hbar\chi\hat{a}^\dagger\hat{a}(|e\rangle\langle e| - |g\rangle\langle g|)$, where $\chi = g_c^2/\Delta$ [29]. This results in a qubit-state-dependent shift by $\pm\chi$ of the resonator frequency when the ABS are in the even manifold, while no shift occurs for the currentless odd manifold. By monitoring the resonator response to a microwave readout tone, the quantum state

of the ABS can thus be determined. However, these frequency shifts must be resolvable with practical measurement integration times. This results in two requirements on the Andreev spectrum. First, the bandwidth of the dispersion of E_A with the superconducting phase difference φ should be maximized, as this sets the scale of the ABS supercurrent operator and thus the value of g_c [7,10]. Second, the minimum of $f_A(\varphi = \pi)$ should be tuned close to f_r, which can be achieved by adjusting the transparency τ of the conduction channel hosting the lowest-energy ABS [Fig. 1(c)] [31]. In particular, the conduction channel must be quasiballistic, such that τ can be tuned close to unity [10].

To achieve a high-τ NWJJ, we used an MBE-grown [001] wurtzite InAs nanowire [Fig. 2(a)] with an epitaxial aluminum (Al) shell [21–23]. The device substrate was composed of intrinsic silicon capped with a 300 nm layer of silicon dioxide. First, the readout resonator ($f_r = 9.066$ GHz, line width $\kappa/2\pi = 9$ MHz) and control structures were patterned by electron-beam lithography and
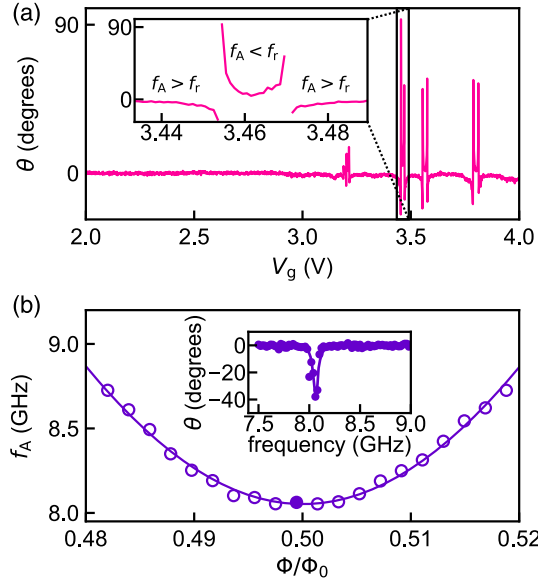
FIG. 3. Control of the Andreev qubit frequency. (a) The average phase θ of the readout tone for a range of V_g values ($\Phi = \Phi_0/2$). Each point was integrated for 1.28 μs. As V_g is varied, transitions in the nanowire come into proximity with the resonator frequency, resulting in avoided crossings. Inset: enlargement of two of these avoided crossings of f_A with the resonator frequency. (b) Inset: Continuous-wave two-tone spectroscopy reveals the qubit transition. The transition frequency f_A is extracted from a best fit to a Lorentzian line shape. Main figure: dependence of f_A on Φ. Solid line is a fit to the short-junction formula for f_A [31].

reactive ion etching of sputtered niobium titanium nitride (NbTiN). Then, the nanowire was deposited using a micromanipulator and the junction was defined by selectively wet etching a 200 nm long section of the Al shell [Fig. 2(a)]. NWJJs of this length have been shown to host ABS with large phase dispersion [22]. The Al leads of the NWJJ were contacted to the rest of the circuit with NbTiN [Fig. 2(b)]. We implemented control over τ via an electrostatic gate voltage V_g [Figs 2(a), 2(d)], and we applied an external flux Φ through a NbTiN loop to phase bias the NWJJ [Fig. 2(c)] [22]. Because the inductance of the NWJJ was much greater than that of the NbTiN loop, $\varphi \simeq 2\pi\Phi/\Phi_0$. In contrast with dc transport measurements, the NWJJ was galvanically isolated from all off-chip circuitry. The large critical fields of NbTiN and thin-film Al make our devices compatible with high magnetic field measurements, enabling future experiments in the topological regime [21,32]. The measurements presented here were performed in a dilution refrigerator with a base temperature of $\sim$30 mK.

We first investigated the effects of V_g and Φ on the device properties. With $\Phi = \Phi_0/2$, we monitored the phase θ of the readout tone (frequency f_r) while sweeping V_g [Fig. 3(a)]. For several ranges of V_g, θ exhibits features consistent with a transition crossing f_r [inset Fig. 3(a)]. We attribute this transition to a gate-controlled Andreev qubit

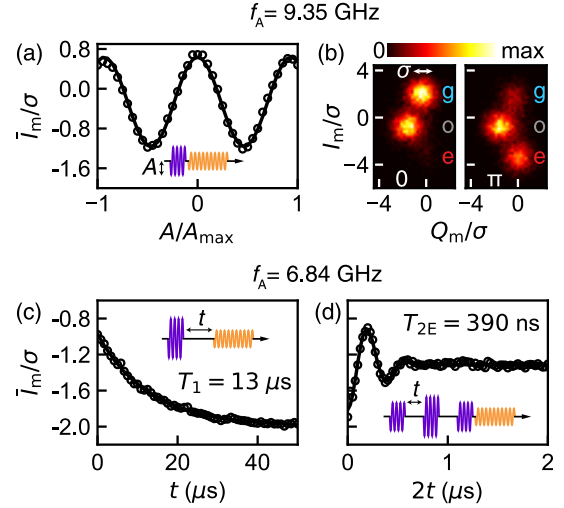FIG. 4. Coherent dynamics of the Andreev qubit. Data are rescaled by the standard deviation σ of the $|g\rangle$ distribution. (a) Rabi oscillations of the Andreev qubit ($f_A = 9.35$ GHz, $\Phi = \Phi_0/2$). A resonant 10 ns square pulse of varying amplitude A was applied to the qubit, followed by a readout pulse at f_r which was integrated for 640 ns. Nominal π and $\pi/2$ qubit rotations were calibrated by fitting the data to a sinusoid (solid line). (b) Histogram of the I_m and Q_m quadratures of the readout tone following no qubit rotation (left) and a π rotation. (c) Energy relaxation of the qubit ($f_A = 6.84$ GHz, $\Phi = \Phi_0/2$). Fitting to a decaying exponential (solid line) yields a time constant $T_1 = 12.8 \pm 0.2$ μs. (d) Coherence of the qubit measured using a Hahn-echo pulse sequence. The phase of the final $\pi/2$ pulse is varied with the delay to introduce oscillations. Solid line is a best fit to a Gaussian decaying sinusoid with time constant $T_{2E} = 390 \pm 10$ ns.

coupled to the readout resonator [Fig. 1(b)]. The abundance of features observed in Fig. 3(a) may be explained by mesoscopic fluctuations of the nanowire conductance [22,23,33], with f_A crossing f_r whenever τ approaches unity [see Fig. 1(c)]. With $f_A(\Phi_0/2)$ tuned below f_r, the frequency of the microwave drive [Fig. 2(d)] was swept to pinpoint the qubit transition [inset Fig. 3(b)]. Repeating this measurement at various flux biases revealed strong dispersion of $f_A(\Phi)$ [Fig. 3(b)], consistent with recent dc and rf measurements of ABS hosted by high-transparency conduction channels in InAs/Al NWJJs [22,23]. Under the simplifying assumption that the coherence length is much greater than the junction length, we therefore apply the simplified formula for the Andreev qubit frequency $f_A(0)\sqrt{1 - \tau\sin^2(\pi\Phi/\Phi_0)}$ [31] and extract $\tau \simeq 0.98$ and $f_A(0) \simeq 60.0$ GHz[$E_A(0) \simeq 124$ μeV]. Measurements of f_A over a wider flux range were impeded by drifts in V_g bias on minute-to-hour timescales, which we attribute to charging effects in the dielectric surrounding the nanowire. While these instabilities made systematic studies requiring long measurement times impossible, they did not inhibit our ability to investigate the fast temporal dynamics of the ABS.
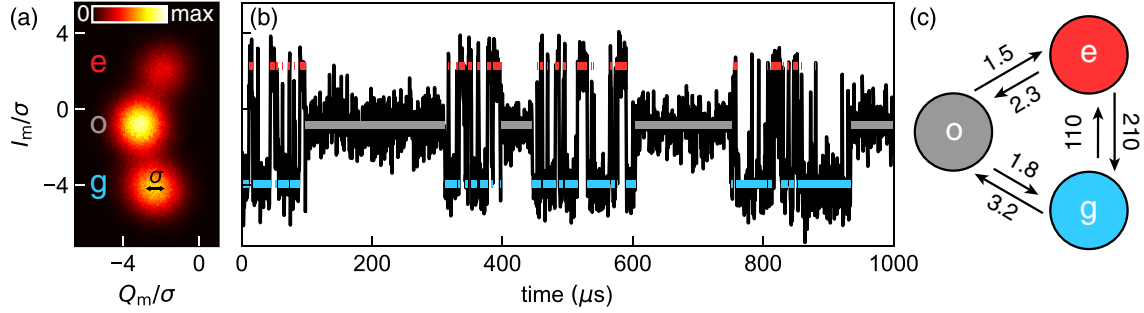
FIG. 5. Dynamics of incoherent transitions between many-body configurations of the ABS. (a) Histogram of the I_m and Q_m quadratures of the readout tone ($f_A = 8.5$ GHz, $\Phi = \Phi_0/2$). Each of the 9.6×10^5 counts corresponds to an integration period of 480 ns. The (I_m, Q_m)-pairs cluster into three Gaussian distributions corresponding to the ABS many-body configurations. Data are rescaled by the standard deviation σ of the $|g\rangle$ distribution. (b) Time evolution of I_m/σ for a sample of the data in (a). State assignments (blue, gray, and red bars) result from a maximum-likelihood estimation to a hidden Markov model. (c) Transition rates in ms^{-1} between the ABS many-body configurations extracted from the hidden Markov model analysis.

Next we probed the coherent dynamics of the f_A transition. Figure 4(a) displays Rabi oscillations of the Andreev qubit at $\Phi = \Phi_0/2$. To verify the effect of the Rabi drive on the ABS, this measurement was performed with high photon number $\bar{n} \sim 100$ and small detuning $\Delta/2\pi = 280$ MHz. In this regime, the integrated quadratures (I_m, Q_m) of the readout pulse clustered into three well-separated Gaussian distributions [Fig. 4(b)] which we attribute to $|g\rangle$, $|e\rangle$, and the odd manifold [10]. As expected, the populations of $|g\rangle$ and $|e\rangle$ are affected by the Rabi drive, while the population of the odd manifold is mainly constant (see Supplemental Material [34], Sec. I). The energy and coherence decay of the Andreev qubit were measured at increased Δ to avoid resonator-induced transitions. The maximum energy relaxation time $T_1 = 12.8 \pm 0.2$ μs was measured with $f_A = 6.84$ GHz [Fig. 4(c)]. At this working point, the Hahn-echo decay time was found to be $T_{2E} = 390 \pm 10$ ns [Fig. 4(d)]. Low-frequency fluctuations in f_A resulted in an immeasurably short Ramsey decay time, which we attribute to the gate-bias instabilities. We note that these energy and coherence decay times are of similar magnitude to those observed in Andreev qubits hosted by superconducting atomic contacts [10], indicating that the loss and dephasing mechanisms may be largely independent of the junction materials.

In addition to studying even-manifold coherence, we observed incoherent transitions between all of the ABS many-body configurations by continuously monitoring the resonator while at small detuning $\Delta/2\pi = -0.5$ GHz and high photon number $\bar{n} \sim 100$ [Figs. 5(a),5(b)]. The transition rates between configurations were extracted using a hidden Markov model algorithm [38]. This analysis assumes that the system possesses three states ($|g\rangle$, $|e\rangle$, and the odd manifold), and that each state i emits (I_m, Q_m) pairs with different (but potentially overlapping) probability distributions $p(I_m, Q_m|i)$. Importantly, $p(I_m, Q_m|i)$ do not need to be known *a priori*. By analyzing the time evolution of (I_m, Q_m), the algorithm yields the most

probable $p(I_m, Q_m|i)$, state assignments [Fig. 5(b)], and transition rates of the system [Fig. 5(c)]. The extracted rates yield a reduced qubit lifetime $T_1 = 3.2 \pm 0.1$ μs, which we attribute to off-resonant driving of the $|g\rangle \leftrightarrow |e\rangle$ transition by the high-power readout tone. This is consistent with the observed nonthermal qubit population [Fig. 5(a)]. In addition, the extracted rates yield a parity-decay timescale $T_{\text{parity}} = 160 \pm 10$ μs (see Supplemental Material [34], Sec. II), which we attribute to spontaneous poisoning of the ABS by nonequilibrium quasiparticles. We note that since $T_{\text{parity}} \gg T_1$, the lifetime of the Andreev qubit was limited by direct $|g\rangle \leftrightarrow |e\rangle$ processes and not by quasiparticle poisoning.

Previous measurements of bound-state poisoning in proximitized semiconducting nanowires have used Coulomb blockade spectroscopy to estimate the rate of quasiparticle relaxation from the superconductor into a bound state [39,40]. Our T_{parity} measurement is distinct in that we directly monitor the parity of the ABS and are therefore sensitive to all parity-breaking processes. To lowest order, the readout tone should not induce parity-breaking transitions, which involve energies on the order of the superconducting gap. However, recent measurements of ABS in superconducting atomic point contacts have shown dependence of T_{parity} on $\bar{n}$ [41]. In future experiments, the dependence of T_{parity} on $\bar{n}$ will be measured using a Josephson parametric converter [42].

In conclusion, we have detected and manipulated the ABS of an InAs NWJJ using a cQED approach. We realized a gate- and flux-tunable Andreev qubit with maximum coherence times $T_1 = 12.8 \pm 0.2$ μs and $T_{2E} = 390 \pm 10$ ns. Moreover, we achieved continuous monitoring of the ABS fermion parity in a NWJJ, revealing that quasiparticle poisoning of the ABS occurred on a timescale $T_{\text{parity}} = 160 \pm 10$ μs. The measurement time of experiments aiming to detect the non-Abelian properties of MBS in a topological nanowire must fall within a certain range. The upper bound is set by T_{parity}, as quasiparticle poisoning of MBS will

decohere superpositions of quantum states with different parity. Conversely, adiabatic manipulation of MBS restricts the lower bound to nanosecond timescales [28]. Therefore, our measured value of T_{parity} leaves an experimentally accessible window for the investigation of Majorana physics.

---

*max.hays@yale.edu

†michel.devoret@yale.edu

[1] A. Andreev, Zh. Eksp. Teor. Fiz. **46,** 1823 (1964).

[2] C. W. J. Beenakker and H. Van Houten, Phys. Rev. Lett. **66,** 3056 (1991).

[3] A. Furusaki and M. Tsukada, Phys. Rev. B **43,** 10164 (1991).

[4] edited by J. Clarke and A. I. Braginski, *The SQUID Handbook* (Wiley, Weinheim, 2004), Vol. 1.

[5] M. H. Devoret and R. J. Schoelkopf, Science **339,** 1169 (2013).

[6] A. Roy and M. Devoret, C.R. Phys. **17,** 740 (2016).

[7] A. Zazunov, V. S. Shumeiko, E. N. Bratus, J. Lantz, and G. Wendin, Phys. Rev. Lett. **90,** 087003 (2003).

[8] N. M. Chtchelkatchev and Y. V. Nazarov, Phys. Rev. Lett. **90,** 226806 (2003).

[9] L. Bretheau, Ç. O. Girit, H. Pothier, D. Esteve, and C. Urbina, Nature (London) **499,** 312 (2013).

[10] C. Janvier, L. Tosi, L. Bretheau, Ç. Ö. Girit, M. Stern, P. Bertet, P. Joyez, D. Vion, D. Esteve, M. F. Goffman *et al.*, Science **349,** 1199 (2015).

[11] M. Zgirski, L. Bretheau, Q. Le Masne, H. Pothier, D. Esteve, and C. Urbina, Phys. Rev. Lett. **106,** 257003 (2011).

[12] A. Zazunov, A. Brunetti, A. L. Yeyati, and R. Egger, Phys. Rev. B **90,** 104508 (2014).

[13] E. M. Levenson-Falk, F. Kos, R. Vijay, L. Glazman, and I. Siddiqi, Phys. Rev. Lett. **112,** 047002 (2014).

[14] J. Aumentado, M. W. Keller, J. M. Martinis, and M. H. Devoret, Phys. Rev. Lett. **92,** 066802 (2004).

[15] A. J. Ferguson, S. E. Andresen, R. Brenner, and R. G. Clark, Phys. Rev. Lett. **97,** 086602 (2006).

[16] J. M. Martinis, M. Ansmann, and J. Aumentado, Phys. Rev. Lett. **103,** 097002 (2009).

[17] M. D. Shaw, R. M. Lutchyn, P. Delsing, and P. M. Echternach, Phys. Rev. B **78,** 024503 (2008).

[18] P. J. de Visser, J. J. A. Baselmans, P. Diener, S. J. C. Yates, A. Endo, and T. M. Klapwijk, Phys. Rev. Lett. **106,** 167004 (2011).

[19] D. Ristè, C. C. Bultink, M. J. Tiggelman, R. N. Schouten, K. W. Lehnert, and L. DiCarlo, Nat. Commun. **4,** 1913 (2013).

[20] W. Chang, S. Albrecht, T. Jespersen, F. Kuemmeth, P. Krogstrup, J. Nygård, and C. Marcus, Nat. Nanotechnol. **10,** 232 (2015).

[21] P. Krogstrup, N. L. B. Ziino, W. Chang, S. M. Albrecht, M. H. Madsen, E. Johnson, J. Nygård, C. M. Marcus, and T. S. Jespersen, Nat. Mater. **14,** 400 (2015).

[22] D. J. van Woerkom, A. Proutski, B. van Heck, D. Bouman, J. I. Väyrynen, L. I. Glazman, P. Krogstrup, J. Nygård, L. P. Kouwenhoven, and A. Geresdi, Nat. Phys. **13,** 876 (2017).

[23] M. F. Goffman, C. Urbina, H. Pothier, J. Nygård, C. M. Marcus, and P. Krogstrup, New J. Phys. **19,** 092002 (2017).

[24] G. de Lange, B. van Heck, A. Bruno, D. J. van Woerkom, A. Geresdi, S. R. Plissard, E. P. A. M. Bakkers, A. R. Akhmerov, and L. DiCarlo, Phys. Rev. Lett. **115,** 127002 (2015).

[25] T. W. Larsen, K. D. Petersson, F. Kuemmeth, T. S. Jespersen, P. Krogstrup, J. Nygård, and C. M. Marcus, Phys. Rev. Lett. **115,** 127001 (2015).

[26] R. M. Lutchyn, J. D. Sau, and S. Das Sarma, Phys. Rev. Lett. **105,** 077001 (2010).

[27] Y. Oreg, G. Refael, and F. von Oppen, Phys. Rev. Lett. **105,** 177002 (2010).

[28] D. Aasen, M. Hell, R. V. Mishmash, A. Higginbotham, J. Danon, M. Leijnse, T. S. Jespersen, J. A. Folk, C. M. Marcus, K. Flensberg *et al.*, Phys. Rev. X **6,** 031016 (2016).

[29] A. Blais, R.-S. Huang, A. Wallraff, S. M. Girvin, and R. J. Schoelkopf, Phys. Rev. A **69,** 062320 (2004).

[30] A. Wallraff, D. I. Schuster, A. Blais, L. Frunzio, R.-S. Huang, J. Majer, S. Kumar, S. M. Girvin, and R. J. Schoelkopf, Nature (London) **431,** 162 (2004).

[31] C. W. J. Beenakker, Phys. Rev. Lett. **67,** 3836 (1991).

[32] V. Mourik, K. Zuo, S. M. Frolov, S. R. Plissard, E. P. A. M. Bakkers, and L. P. Kouwenhoven, Science **336,** 1003 (2012).

[33] H. Ehrenreich and D. Turnbull, *Advances in Research and Applications: Semiconductor Heterostructures and Nanostructures* (Academic Press, New York, 1991), Vol. 44.

[34] See Supplemental Material at http://link.aps.org/supplemental/10.1103/PhysRevLett.121.047001 for further analysis of the ABS dynamics, which includes Refs. [35–37].

[35] E. M. Purcell, Phys. Rev. **69,** 681 (1946).

[36] U. Vool, I. M. Pop, K. Sliwa, B. Abdo, C. Wang, T. Brecht, Y. Y. Gao, S. Shankar, M. Hatridge, G. Catelani *et al.*, Phys. Rev. Lett. **113,** 247001 (2014).

[37] A. Bhattacharyya, Bull. Calcutta Math. Soc., **35,** 99 (1943).

[38] W. H. Press, S. A. Teukolsky, W. T. Vetterling, and B. P. Flannery, *Numerical Recipes in C++* (Cambridge University Press, Cambridge, 2015).

[39] A. P. Higginbotham, S. M. Albrecht, G. Kiršanskas, W. Chang, F. Kuemmeth, P. Krogstrup, T. S. Jespersen,

J. Nygård, K. Flensberg, and C. M. Marcus, Nat. Phys. **11**, 1017 (2015).

[40] S. M. Albrecht, E. B. Hansen, A. P. Higginbotham, F. Kuemmeth, T. S. Jespersen, J. Nygård, P. Krogstrup, J. Danon, K. Flensberg, and C. M. Marcus, Phys. Rev. Lett. **118**, 137701 (2017).

[41] C. Janvier, Ph. D. thesis, Université Paris-Saclay, 2016.

[42] N. Bergeal, F. Schackert, M. Metcalfe, R. Vijay, V. E. Manucharyan, L. Frunzio, D. E. Prober, R. J. Schoelkopf, S. M. Girvin, and M. H. Devoret, Nature (London) **465**, 64 (2010).